Polyaromatics

How to cite:
International Edition: doi.org/10.1002/anie.202300571
German Edition: doi.org/10.1002/ange.202300571

Tetrazo[1,2-*b*]indazoles: Straightforward Access to Nitrogen-Rich Polyaromatics from *s*-Tetrazines

Ahmad Daher[+], Asmae Bousfiha[+], Iogann Tolbatov, Clève D. Mboyi, Hélène Cattey, Thierry Roisnel, Paul Fleurat-Lessard, Muriel Hissler, Jean-Cyrille Hierso, Pierre-Antoine Bouit,* and Julien Roger**

Abstract: The straightforward access to a new class of aza-polyaromatics is reported. Starting from readily available fluorinated s-tetrazine, a cyclization process with azide leads to the formation of an unprecedented tetrazo[1,2-*b*]indazole or a bis-tetrazo[1,2-*b*]indazole (*cis* and *trans* conformers). Based on the new nitrogen core, further N-directed palladium-catalyzed *ortho*-C–H bond functionalization allows the introduction of halides or acetates. The physicochemical properties of these compounds were studied by a joint experimental/theoretical approach. The tetrazo[1,2-*b*]indazoles display solid-state π-stacking, low reduction potential, absorption in the visible range up to the near-infrared, and intense fluorescence, depending on the molecular structure.

Introduction

N-heterocycles are important building blocks for biomedical, agrochemical applications as well as in material sciences. In particular, *N*-containing polyaromatics are interesting in the field of optoelectronics/photonics as their reactivity, their aromaticity, their self-assembly and ultimately their physicochemical properties highly depend on the *N*-substituents and the nature of the heterocycle.[1] A successful strategy to further afford molecular diversity and fine-tune the optoelectronic properties is to increase the *N*-content in the heterocycles to enhance the electron affinity demonstrated by the development of the polyazapentalenes (Scheme 1).[2,3] Another representative example of azaheterocycle for optoelectronics is the *s*-tetrazine (Tz, 1,2,4,5-tetrazine, see **A**, Scheme 1) that appears both as a highly versatile fluorophore and a redox switchable unit allowing for example to prepare efficient electrofluorochromic devices.[4] Increasing the *N*-content and rigidifying the structure such in heptazine allowed to reinforce the electron affinity and to use them for example as photocatalysts.[5]

In such context, any innovative synthetic approach allowing the preparation and straightforward functionalization of unprecedented conjugated *N*-heterocycles is highly desirable.[6]

In this context, we envisioned using intramolecular azido-cyclization[7] from adequately functionalized tetrazines (such as **B**, Scheme 1, bottom) to produce unprecedented N-rich polyaromatics (either symmetric tetrazo[1,2-*b*]indazole **D** or dissymmetric **C**, Scheme 1, bottom).[8] Such scaffold will display a polyaromatic skeleton featuring five or six N atoms and will thus possess strong electron affinity, in addition to favorable optical properties typical of polyaromatic systems. Furthermore, we envisage to use *N*-directed C–H activation to easily post-

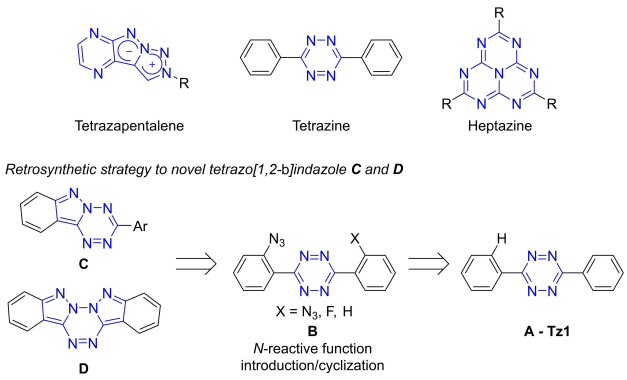

Scheme 1. Classical *N*-rich heteroaromatics in the field of optoelectronics/photonics (top) and retrosynthesis strategy to novel tetrazo[1,2-*b*]indazoles **C** and **D** (bottom, *this work*).

[*] A. Daher,[+] Dr. A. Bousfiha,[+] Dr. I. Tolbatov, Dr. C. D. Mboyi, Dr. H. Cattey, Prof. Dr. P. Fleurat-Lessard, Prof. Dr. J.-C. Hierso, Dr. J. Roger
Institut de Chimie Moléculaire de l'Université de Bourgogne, UMR CNRS 6302 - Université Bourgogne (UB)
9, avenue Alain Savary 21078 Dijon (France)
E-mail: Paul.Fleurat-Lessard@u-bourgogne.fr
julien.roger@u-bourgogne.fr
Dr. T. Roisnel, Dr. M. Hissler, Dr. P.-A. Bouit
CNRS, ISCR-UMR 6226, Univ Rennes
35000 Rennes (France)
E-mail: pierre-antoine.bouit@univ-rennes1.fr
[+] These authors contributed equally to this work.

functionalize the polyaromatic scaffold. The mechanism of the cyclization was investigated computationally. Finally, the optical and redox properties of these new derivatives were studied to highlight their potential applications in optoelectronics.

Results and Discussion

Following our previous works,[9] the catalytic copper insertion of azide in *ortho*-position on the brominated tetrazine (**Tz-Br**) was achieved in presence of 20 mol % of $[Cu(OAc)_2.H_2O]$, TMEDA as the ligand with azidotrimethylsilane at 50 °C in 1,4-dioxane.[9b] When the reaction was performed at 120 °C, the corresponding 6-aryltetrazo[1,2-*b*]indazole **2a** was formed with low yield (20 %) (Scheme 2 and Scheme S1). After optimizations, we noticed that 3-(2-fluorophenyl)-6-phenyl tetrazine **1a** was a more valuable starting material for such transformation (Scheme 2, top and Table S1 and S2). Indeed, in the presence of 3 equivalents of NaN_3 in DMF after one hour using microwave irradiations (μw, 200 W), **2a** was obtained in 70 % isolated yield. Under similar conditions, the 3,6-(2-fluorophenyl)-6-phenyl tetrazine **1b** gives **2b** with 43 % isolated yields.

The structure of **2b** was unambiguously characterized by X-ray diffraction (Scheme 2, bottom). Compound **2b** crystallizes in the $P2_1$ space group of the monoclinic system. The unit cell consists in two crystallographically independent molecules (see ESI RX).[10] The polyaromatic platform is mostly planar (maximal deviation from the mean plane: 0.10 Å). The *ortho*-fluorophenyl ring is tilted of ca. 39° from the tetrazo[1,2-*b*]indazole platform. At the intermolecular level, two molecules interact through the simultaneous π-interaction of one fluorophenyl and a tetrazine ring (d = 3.6 Å and 3.4 Å) thus forming a network of infinite π-columns, interesting for further solid-state charge transport applications (Figure S13).

Regarding the cyclization mechanism, the formation of 3-(phenyl)-[1,2,4,5]-tetrazo[1,2-*b*]indazole **2a** starts from **Tz-N_3** functionalized at the *ortho*-carbon of the benzene ring (Figure 1). Two mechanisms are envisioned according to literature: *i*) the approach of the azide nitrogen bound to carbon toward the nitrogen of the Tz core (Figure 1, blue pathway),[11] *ii*) a Diels–Alder reaction with an attack of two azide nitrogens toward the Tz, concerted with the release of a N_2 fragment (Figure 1, black pathway).[12] The formation of a nitrene intermediate, usually stabilized by complexation to a metal, was also considered.[7,13,14] However, all our attempts to optimize the nitrene intermediate led to the direct formation of the cyclization product **2a**. The two reaction pathways are under kinetic control, both being strongly exergonic (−63.1 kcal mol^{-1}). The activation barriers of the two pathways are 34.1 and 46.2 kcal mol^{-1} respectively, thus suggesting that the direct addition of azide is substantially favored over the Diels–Alder path.

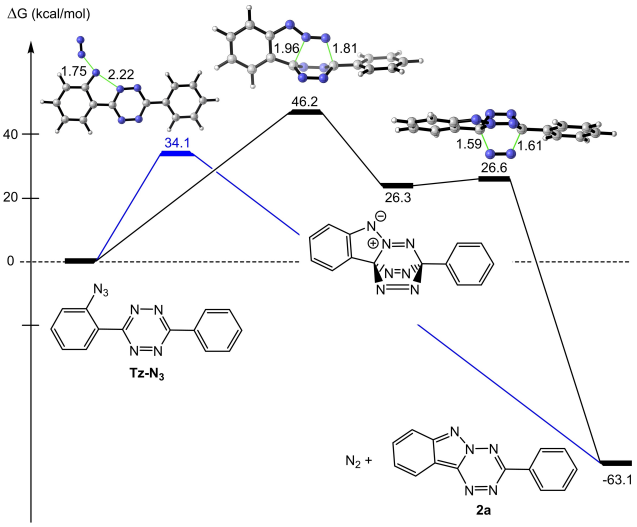

Figure 1. Formation of the 3-(phenyl)-[1,2,4,5]-tetrazo[1,2-*b*]indazole **2a**. Values represent Gibbs free energies in kcal mol^{-1}.

We envisaged to use a *N*-directed C–H activation strategy to easily post-functionalize these novel poly *N*-containing scaffold. To evaluate its ability to be post-functionalized, the new tetrazo[1,2-*b*]indazole core **2a** was employed as a *N*-directing group in the electrophilic palladium-catalyzed C–H functionalization. C–X (X = Br, Cl and F) and C–O bonds were successfully formed at the *ortho*-position of the aryl of the tetrazo[1,2-*b*]indazole by Pd catalysis (Table 1 and Table S4 to S7). Monofluorination or difluorination occurred in the presence of $[Pd(dba)_2]$, *N*-fluorobenzenesulfonimide (NFSI) as the electrophilic reagent in trifluoromethyl benzene ($PhCF_3$) with 56 % and 82 % for **2b** and **2c** respectively (Table 1, entries 1–2). Bromination and chlorination successfully achieved, and **2d**, **2e** and **2f** were obtained in 66 %, 85 % and 40 % isolated yields, respectively, in the presence of the corresponding *N*-halosuccinimide (Table 1, entries 3–5). Acetoxylation takes place in the presence of $[Pd(OAc)_2]$ with phenyl iodane diacetate (PIDA) in HOAc in only 10 minutes under microwave irradiation and furnished **2e** and **2f** in 50 % and 70 % isolated yields, respectively (Table 1, entries 6–7). Unequal functionalization was also achieved (Table 1, entry 8), starting from the 3-(2-fluorophenyl)-[1,2,4,5]-tetrazo-[1,2-*b*]indazole **2b**, bromination toward **2i** was obtained in good yield (80 %). Again, **2c–i** were fully characterized by multinuclear

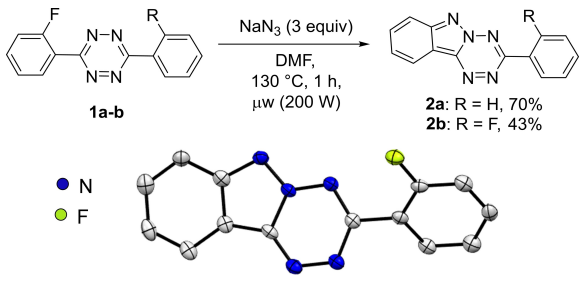

Scheme 2. Cyclization reaction to 3-(aryl)-[1,2,4,5]-tetrazo[1,2-*b*]indazole **2a–b** and crystallographic structure of **2b**.

Table 1: *N*-directed palladium-catalyzed C–H bond functionalization of **2a**.[a]

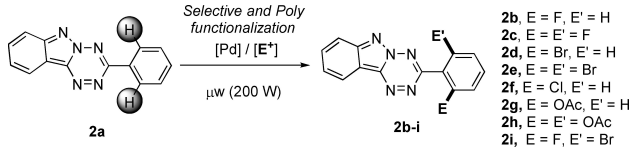

Entry	[Pd] (mol%)	Oxidant (equiv)	Solvent [0.04 M]	Time [min]	**2b–i** [%]
1	$Pd(dba)_2$ (20)	NFSI (2.0)	$PhCF_3$	10	**2b**: 56
2	$Pd(dba)_2$ (20)	NFSI (5.0)	$PhCF_3$	30	**2c**: 82
3	$Pd(OAc)_2$ (10)	NBS (1.0)	CH_3NO_2	10	**2d**: 66
4	$Pd(OAc)_2$ (10)	NBS (2.0)	CH_3NO_2	10	**2e**: 85
5	$Pd(dba)_2$ (20)	NCS (3.0)	AcOH	10	**2f**: 40
6	$Pd(OAc)_2$ (15)	PIDA (1.0)	AcOH	10	**2g**: 50
7	$Pd(OAc)_2$ (20)	PIDA (2.2)	AcOH	10	**2h**: 70
8[b]	$Pd(OAc)_2$ (10)	NBS (1.0)	CH_3NO_2	10	**2i**: 80

[a] Conditions: 3-(aryl)-[1,2,4,5]-tetrazo[1,2-*b*]indazole **2a** (1 equiv), [Pd] (10–20 mol%), oxidant (1.0 to 4.0 equiv), solvent (0.04 M), 110 °C, 200 W, under air. Isolated yield. [b] From **2b**.

NMR, high resolution mass spectrometry and X-ray diffraction in the case of **2d** (see ESI RX). These examples nicely illustrate that the tetrazo-[1,2-*b*]indazole core can be easily and efficiently post-functionalized using *N*-directed C–H bond activation.

Due to the symmetry of the Tz core, the formation of bis-tetrazo[1,2-*b*]indazole **3** was also envisaged through a double cyclization (Scheme 3, and Table S2 and S3).

Thus, 3,6-bis(2-fluorophenyl)-[1,2,4,5]-tetrazine **1b** in the presence of NaN_3 (3 equiv) in DMF was converted in 34% isolated yield of the corresponding bis-tetrazo[1,2-*b*]indazole **3** as a mixture of *cis* and *trans* isomers.[15] Starting from 3-(2-fluorophenyl)-tetrazo[1,2-*b*]indazole **2b** the cyclization allowed to isolate (**3-*cis*** + **3-*trans***) in 44% yield. In these reactions, various other products were observed in the crude mixture. While **3-*cis*** displays good solubility in organic solvents, the low solubility of the other products (including **3-*trans***) made difficult the full rationalization of the reaction. Nevertheless, we were able to isolate and characterize **3-*cis*** and **3-*trans***, by multinuclear NMR and high resolution mass spectrometry, X-ray diffraction in the case of **3-*cis*** (see below). In addition, despite their high *N*-content, compound **3** (as well as **2a–b**) displays a good thermal stability, as evidenced by thermogravimetric analysis (Figure S1).

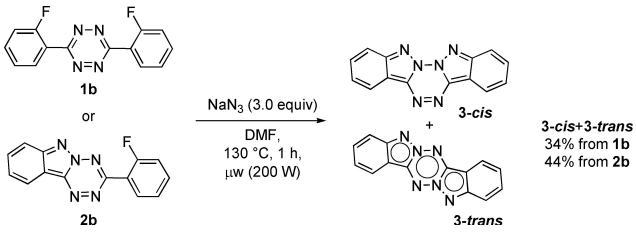

Scheme 3. Reaction toward bis-[1,2,4,5]-tetrazo[1,2-*b*]indazole **3**.

The mechanism for the second cyclization was also investigated at DFT level (Figure 2). DFT calculations concluded that the most favorable reaction route for the formation of the bis-[1,2,4,5]-tetrazo[1,2-*b*]indazole **3** follows the same mechanism as previously described for 3-(phenyl)-[1,2,4,5]-tetrazo[1,2-*b*]indazole **2a**, *i.e.*, the cyclization of azide-functionalized complex upon approach of the azide nitrogen toward the tetrazine nitrogen. If the second cyclization of tetrazoindazole occurs on the opposite side of the molecule, a *trans*-bis-[1,2,4,5]-tetrazo-[1,2-*b*]indazole **3-*trans*** is produced. Conversely, a *cis*-bis-[1,2,4,5]-tetrazo[1,2-*b*]indazole **3-*cis*** is formed when the second cyclization takes place on the same side as the first one. According to our computations, the formation of the *trans* isomer is favored by 1.1 kcal mol^{-1} ($\Delta G^{\ddagger}(cis) = 35.5$ kcal mol^{-1} vs $\Delta G^{\ddagger}(trans) = 34.4$ kcal mol^{-1}). At 130 °C, this should lead to a 80:20 *trans/cis* ratio. However, as previously mentioned, the low solubility of most products made it difficult to quantitatively isolate both isomers.

The structure of **3-*cis*** was unambiguously characterized by X-ray diffraction (Figure 3 and ESI RX). **3-*cis*** crystallizes in the $P2_1$ space group of the monoclinic system and the unit cell consists in two crystallographi-

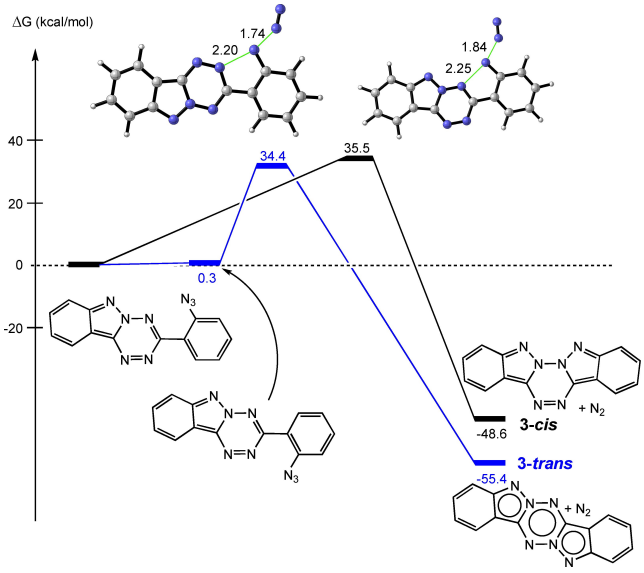

Figure 2. Gibbs free energy profile (in kcal mol^{-1}) for the formation of *cis*- and *trans*-bis-[1,2,4,5]-tetrazo[1,2-*b*]indazole **3** from 3-(2-fluorophenyl)-[1,2,4,5]-tetrazo[1,2-*b*]indazole **2b** after substitution of fluorine by the azide.

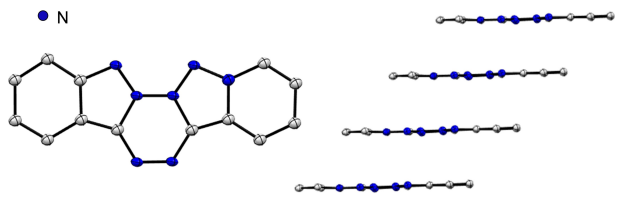

Figure 3. X-ray crystallographic structure of **3-*cis*** and view of the infinite columns.

cally independent molecules of **3-*cis***. The polyaromatic platform is fully planar (maximal deviation from the mean plane: 0.05 Å). The nucleus-independent chemical shift $NICS(0)_{iso}$ values reveal that the newly formed indazole ring is highly aromatic (≈−14/-16) in all cases (**2–3-*cis*/*trans***). It also shows that the aromaticity in the central Tz ring increases from the slightly antiaromatic **Tz1** (+2.0) to **2a** (−3.5), **3-*cis*** (−5.2) and **3-*trans*** (−7.8) (Figure S-Th-1). This nicely illustrates the strong modifications of the electronic properties in these heterocycles, which will impact their physico-chemical properties. Finally, at the intermolecular level, π–π interactions between **3-*cis*** platforms take place (π–π distances, 3.30 Å, Figure 3) affording infinite π columns. Such supramolecular organization is highly promising for further optoelectronic applications related to solid state charge transport.

The spectroscopic properties of **2–3** are investigated in diluted CH_2Cl_2 solutions ($c = 5.10^{-6}$ mol L^{-1}, Figure 4, and Figures S2 to S8, Table S8). The tetrazo[1,2-*b*]indazole **2a–i** all display large absorption with moderate extinction coefficient in the visible range (λ_{abs}(**2a**) = 435 nm; ε_{max} = 2300 L mol^{-1} cm^{-1}). Such transition is assigned to π–π* transition in the tetrazo[1,2-*b*]indazole core (see Figure S-Th-2). The absorption appears blue-shifted compared to the Tz precursors (for example λ_{abs}(**Tz1**) = 542 nm).[16] The

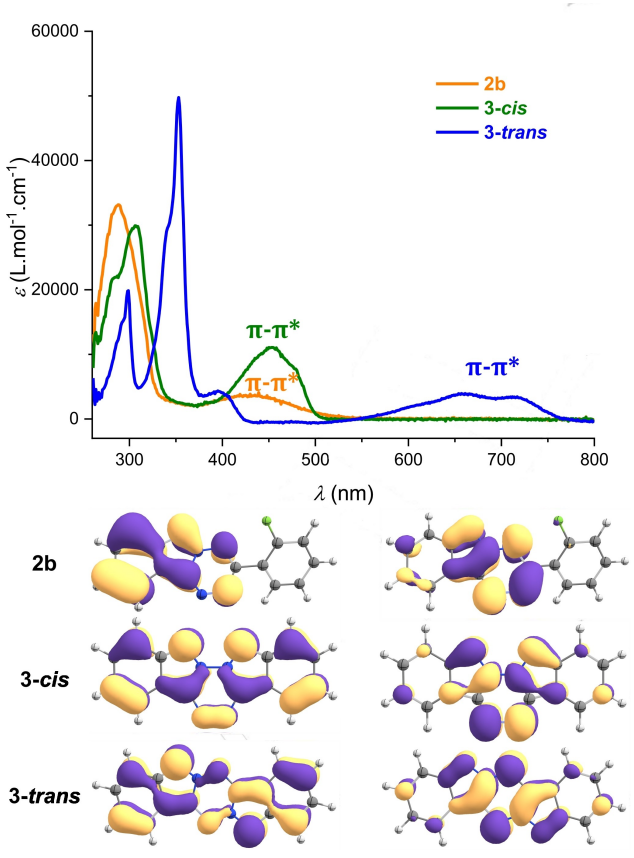

Figure 4. UV/Vis absorption of **2b** (orange), **3-*trans*** (blue) and **3-*cis*** (green) in DMSO (10^{-5} M) (top). HOMO (left) and LUMO (right) of **2b** (top), **3-*cis*** (middle) and **3-*trans*** (down) at the B3LYP/6-311++G(d,p) level. Contour isovalue is 0.03 a.u.

effect of post-functionalization has limited impact on the optical properties (see Figure S2) and is nicely corroborated by TD-DFT (Figure S-Th-4). This is easily explained as the modifications are performed in *ortho*-position of the lateral Ph ring that is not involved either in HOMO nor LUMO (see Figure 4 bottom and Figure S-Th-3). As expected, the presence of the second fused cycle in **3-*cis*** red-shifts the UV/Vis absorption (independently of the solvent, see Figure S-4) with an increase of the molar absorption (λ_{abs}(**3-*cis***) = 455 nm; ε_{max} = 7200 L mol^{-1} cm^{-1}). Here also, the transition is assigned to π-π* transition in the bis-tetrazo[1,2-*b*]indazole core (see Figure S-Th-6). The red shift is even more pronounced for **3-*trans*** (λ_{abs}(**3-*trans***) = 712 nm, recorded in DMSO) which displays the peculiar mesoionic structure and absorption up to the near infrared.[17] Indeed, **3-*trans*** displays a destabilized HOMO compared to **3-*cis*** (Figure 4 bottom) and thus a smaller gap in this case. This absorption in the red part of the visible range is nicely fitted by TD-DFT (Figure S-Th-5) and is a characteristic signature of the **3-*trans*** scaffold.

The molecular structure of the bis-tetrazo[1,2-*b*]indazole also has a dramatic impact on the luminescence. The tetrazo[1,2-*b*]indazoles **2a–i** do not not luminesce (even at 77 K). Interestingly, on the *s*-Tz family, the absence of luminescence was correlated with the occurrence of π–π* transition (contrary to the n-π* that leads to strong luminescence).[16] On the contrary, **3-*cis*** displays intense and structured luminescence (Figure S6) at 532 nm (φ = 0.52 in DCM) with a lifetime of 7 ns, typical for an organic fluorescent emitter. Such intense fluorescence, is independent of the solvent (Figure S-7) and displays a moderate Stokes shift (σ = 3180 cm^{-1} in DCM). These observations, associated with the π-π* nature of the transition make that the **3-*cis*** behaves more like a polycyclic aromatic hydrocarbon than a "Tz like" derivative. It should be noted that **3-*trans*** does not show any luminescence in diluted DMSO, which is consistent with the energy gap law, as **3-*trans*** absorbs until the near infrared. The electrochemical behavior of **2a–i** and **3** were investigated by cyclic voltammetry in dichloromethane or DMF solutions (see Figure S9 to S12). Tetrazo[1,2-*b*]indazoles **2a–g** display one reversible reduction wave at low potential in CH_2Cl_2 (for example E_{red}(**2a**) = −1.29 V vs Fc) which is in the range of diphenyl-tetrazine,[18] a building block recognized for its electron-accepting properties.[4] Even if the effect of *ortho*-substitution in **2b–i** is weak, the presence of two electron-withdrawing groups in **2g–h** allows increasing the reduction potential by 50 mV. The fusion of a second indazole in **3-*cis*** decreases the reduction potential by ≈150 mV (E_{red}(**3-*cis***) = −1.45 V vs Fc in CH_2Cl_2).

The reduction potential is similar in DMF, however the reversibility is decreased (see Figure S9). On the contrary, **3-*trans*** is reduced at higher potential (E_{red} = −1.17 V vs Fc in DMF) and also displays an oxidation wave (E_{ox} = +0.75 V vs Fc) illustrating its small HOMO–LUMO gap, in agreement with the optical properties and the DFT simulations. Importantly **2–3** are reduced in the same range of potential than the corresponding Tz

recorded in the same conditions (E_{red} (**Tz1**) = −1.33 V vs Fc). This confirms that the tetrazo[1,2-*b*]indazoles are polycyclic compounds with high electron affinity that can thus be used for example as electron transport materials in opto-electronic devices.

Conclusion

A new class of aza-polyaromatics, namely tetrazo[1,2-*b*]indazole **2**–**3**, is synthesized by azide cyclization from *s*-tetrazine. The mechanism of this unprecedented cyclization was studied computationally. Based on the new nitrogen core, further *N*-directed palladium-catalysed *ortho*-C–H bond functionalization was performed. The polycycle displays π-stacking in the solid-state. Compounds **2**–**3** display low reduction potential, absorption in the visible range up to the near infrared and intense fluorescence in the case of bis-tetrazo[1,2-*b*]indazole **3**. Thanks to its straightforward synthetic access and easy tunability, the tetrazo[1,2-*b*]indazole scaffold thus appears as an emerging class of organic semi-conductor that can be used in various photonic or optoelectronic applications (solar cells, OFET).

Acknowledgements

This work was supported by the CNRS, Conseil Régional de Bourgogne (PARI and FEDER programs), by the COMUE UBFC (ISITE UB180013.MUB. IS_SmarTZ; R. J., I. T. and PhD grant for A. D.), by the ANR JCJC program 2018 FITFUN (ANR-18-CE07-0015; R. J.) and ANR Pi-Aza (ANR-21-CE07-0024-01, P.-A. B., A. B.). Calculations were performed using HPC resources from DSI-CCUB at the Université de Bourgogne and from GENCI- (CINES and IDRIS, Grant 2017-A0030807259, P. F.-L.). Thanks is due to the PACSMUB platform for analyses (SATT SAYENS) especially M.-J. Penouilh and Q. Bonnin.

Conflict of Interest

The authors declare no conflict of interest.

Data Availability Statement

The data that support the findings of this study are available in the supplementary material of this article.

Keywords: Chromophores · Palladium · Redox Properties · Tetrazines · Tetrazo[1,2-*b*]Indazoles

[1] a) S. M. Draper, D. J. Gregg, E. R. Schofield, W. R. Browne, M. Duati, J. G. Vos, P. Passaniti, *J. Am. Chem. Soc.* **2004**, *126*, 8694; b) D. Reger, K. Schöll, F. Hampel, H. Maid, N. Jux, *Chem. Eur. J.* **2021**, *27*, 1984.

[2] See for instance: a) K. Namba, A. Osawa, S. Ishizaka, N. Kitamura, K. Tanino, *J. Am. Chem. Soc.* **2011**, *133*, 11466; b) D. Sirbu, J. Diharce, I. Martinic, N. Chopin, S. V. Eliseeva, G. Guillaumet, S. Petoud, P. Bonnet, F. Suzenet, *Chem. Commun.* **2019**, *55*, 7776; c) M. Daniel, M. A. Hiebel, G. Guillaumet, E. Pasquinet, F. Suzenet, *Chem. Eur. J.* **2020**, *26*, 1525.

[3] S. Gutierrez, A. Arnault, V. Ferreira, A. Artigas, D. Hagebaum-Reignier, Y. Carissan, Y. Coquerel, M.-A. Hiebel, F. Suzenet, *J. Org. Chem.* **2022**, *87*, 13653.

[4] a) G. Clavier, P. Audebert, *Chem. Rev.* **2010**, *110*, 3299; b) H. Wu, N. K. Devaraj, *Acc. Chem. Res.* **2018**, *51*, 1249; c) P. Audebert, F. Miomandre, *Chem. Sci.* **2013**, *4*, 575.

[5] P. Audebert, E. Kroke, C. Posern, S. H. Lee, *Chem. Rev.* **2021**, *121*, 2515.

[6] a) K. Schwärzer, S. K. Rout, D. Bessinger, F. Lima, C. E. Brocklehurst, K. Karaghiosoff, T. Bein, P. Knochel, *Chem. Sci.* **2021**, *12*, 12993; b) E. Yen-Pon, P. A. Champagne, L. Plougastel, S. Gabillet, P. Thuéry, M. Johnson, G. Muller, G. Pieters, F. Taran, K. N. Houk, D. Audisio, *J. Am. Chem. Soc.* **2019**, *141*, 1435; c) R. Heckerschoff, S. Maier, T. Wurm, P. Biegger, K. Bröder, P. Krämer, M. T. Hoffmann, L. Eberle, J. Stein, F. Rominger, M. Rudolph, J. Freundenberg, A. Dreuw, A. S. K. Hashmi, U. H. F. Bunz, *Chem. Eur. J.* **2022**, *28*, e202104203; d) A. Suleymanov, A. Ruggi, O. Planes, A. S. Chauvin, R. Scopelliti, F. Fadaei Tirani, A. Sienkiewicz, A. Fabrizio, C. Corminboeuf, K. Severin, *Chem. Eur. J.* **2019**, *25*, 6718; e) P. Karak, C. Dutta, T. Dutta, A. L. Koner, J. Choudhury, *Chem. Commun.* **2019**, *55*, 6791.

[7] a) G. Soderberg, *Curr. Org. Chem.* **2000**, *4*, 727; b) F. Xie, X. Li, *Angew. Chem. Int. Ed.* **2013**, *52*, 11862; *Angew. Chem.* **2013**, *125*, 12078; c) Q.-Z. Zheng, P. Feng, Y.-F. Liang, N. Jiao, *Org. Lett.* **2013**, *15*, 4262.

[8] For pyrido[1,2-*b*]indazole synthesis, see: a) P. Tapolcsányi, G. Krajsovszky, R. Ando, P. Lipcsey, G. Horvath, P. Matyus, Z. Riedl, G. Hajos, B. U. W. Maes, G. L. F. Lemiere, *Tetrahedron* **2002**, *58*, 10137; b) R. A. Abramovitch, J. Kalinowski, *Heterocycl. Chem.* **1974**, 857; c) M. V. Méndez, S. O. Simonetti, T. S. Kaufman, A. B. Bracca, *New J. Chem.* **2019**, *43*, 10803; d) J. Balog, Z. Riedl, G. Hajós, *Tetrahedron Lett.* **2013**, *54*, 5338; e) D. Limbach, M. Geffe, H. Detert, *ChemistrySelect* **2018**, *3*, 249–252; f) T. V. Nykaza, T. S. Harrison, A. Ghosh, R. A. Putnik, A. T. Radosevich, *J. Am. Chem. Soc.* **2017**, *139*, 6839.

[9] a) C. Testa, E. Gigot, S. Genc, R. Decreau, J. Roger, J.-C. Hierso, *Angew. Chem. Int. Ed.* **2016**, *55*, 5555; *Angew. Chem.* **2016**, *128*, 5645; b) C. D. Mboyi, C. Testa, S. Reeb, S. Genc, H. Cattey, P. Fleurat-Lessard, J. Roger, J.-C. Hierso, *ACS Catal.* **2017**, *7*, 8493; c) C. D. Mboyi, A. Daher, N. Khirzada, C. H. Devillers, H. Cattey, P. Fleurat-Lessard, J. Roger, J.-C. Hierso, *New J. Chem.* **2020**, *44*, 15235; d) H. Xiong, Y. Gu, S. Zhang, F. Lu, Q. Ji, L. Liu, P. Ma, G. Yang, W. Hou, H. Xu, *Chem. Commun.* **2020**, *56*, 4692; e) C. D. Mboyi, D. Vivier, A. Daher, P. Fleurat-Lessard, H. Cattey, C. H. Devillers, C. Bernhard, F. Denat, J. Roger, J.-C. Hierso, *Angew. Chem. Int. Ed.* **2020**, *59*, 1149; *Angew. Chem.* **2020**, *132*, 1165.

[10] Deposition numbers 2234376. (**2b**), 2234376. (**3-*cis***), and 2234377 (**2d**) contain the supplementary crystallographic data for this paper. These data are provided free of charge by the joint Cambridge Crystallographic Data Centre and Fachinformationszentrum Karlsruhe Access Structures service.

[11] B. J. Stokes, C. V. Vogel, L. K. Urnezis, M. Pan, T. G. Driver, *Org. Lett.* **2010**, *12*, 2884.

[12] a) Y. F. Yang, Y. Liang, F. Liu, K. N. Houk, *J. Am. Chem. Soc.* **2016**, *138*, 1660; b) A. V. Polezhaev, D. M. Beagan, A. C. Cabelof, C. H. Chen, K. G. A. Caulton, *Dalton Trans.* **2018**, *47*, 5938.

[13] R. A. Abramovitch, K. A. H. Adams, *Can. J. Chem.* **1961**, *39*, 2516.
[14] B. J. Stokes, K. J. Richert, T. G. Driver, *J. Org. Chem.* **2009**, *74*, 6442.
[15] Note that **3-*trans*** is a mesoionic derivative, with electronic structure reminiscent of the azapentalene skeleton (see Figure S-Th-9). See also ref. [2].
[16] Y.-H. Gong, F. Miomandre, R. Méallet-Renault, S. Badré, L. Galmiche, J. Tang, P. Audebert, G. Clavier, *Eur. J. Org. Chem.* **2009**, 6121.
[17] For solubility reasons, the comparison of spectroscopic and redox properties between **3-*cis*** and **3-*trans*** was made in DMSO or DMF. Note that the reversibility of the redox processes is lower in DMSO compared to DCM, see the ESI.
[18] H. Fischer, T. Müller, I. Umminger, F. A. Neugebauer, H. Chandra, M. C. R. Symons, *J. Chem. Soc. Perkin Trans. 2* **1988**, 413.

Manuscript received: January 12, 2023
Accepted manuscript online: January 29, 2023
Version of record online: ■■, ■■

Research Articles

Polyaromatics

A. Daher, A. Bousfiha, I. Tolbatov, C. D. Mboyi, H. Cattey, T. Roisnel, P. Fleurat-Lessard,* M. Hissler, J.-C. Hierso, P.-A. Bouit,* J. Roger* _____ **e202300571**

Tetrazo[1,2-*b*]indazoles: Straightforward Access to Nitrogen-Rich Polyaromatics from *s*-Tetrazines

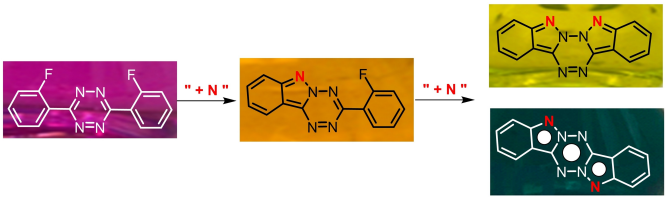

The straightforward access to a new class of aza-polyaromatics is reported starting from fluorinated *s*-tetrazine. The tetrazo[1,2-b]indazoles display solid-state π-stacking, low reduction potential, absorption in the visible range up to the near-infrared and intense fluorescence, depending on the molecular structure.